Origin of perpendicular magnetic anisotropy in epitaxial Pd/Co/Pd(111) trilayers

A. V. Davydenko,* A. G. Kozlov, A. V. Ognev, M. E. Stebliy, A. S. Samardak, K. S. Ermakov, A. G. Kolesnikov, and L. A. Chebotkevich

Laboratory of Thin Film Technologies, School of Natural Sciences, Far Eastern Federal University, Vladivostok, 690950, Russian Federation

(Received 23 November 2016; revised manuscript received 12 January 2017; published 28 February 2017)

Perpendicular magnetic anisotropy in epitaxial Pd/Co/Pd(111) trilayered films grown on Si(111) substrate was investigated. Contributions to perpendicular magnetic anisotropy from the bottom and top Co/Pd interfaces were deduced by replacement of Pd layers by Cu layers and comparative analysis of the magnetic anisotropy in the samples. Perpendicular magnetic anisotropy in Pd/Co/Pd films was induced both by interface electronic effects and by stress caused by lattice mismatch between Pd and Co. Due to asymmetry of the stress in the Co film, the contribution to magnetic anisotropy induced by the bottom Co/Pd interface was stronger than that induced by the top Pd/Co interface. The energy of the perpendicular magnetic anisotropy and asymmetrical contributions from the bottom Co/Pd and top Pd/Co interfaces to anisotropy in Pd/Co/Pd trilayers strongly depend on the thickness of the bottom and top Pd layers and may be precisely controlled. The roughness of the interfaces does not have a large influence on the energy of perpendicular magnetic anisotropy in this system.

DOI: 10.1103/PhysRevB.95.064430

I. INTRODUCTION

Ultrathin magnetic films with perpendicular magnetic anisotropy (PMA) and spin-orbit coupling are of high scientific interest due to their application in novel types of high-density magnetic memory and information processing devices [1–4]. In this respect, an epitaxial Co/Pd(111) multilayered system is attractive because it demonstrates strong PMA [5] and high thermal stability [6]. Investigation of the epitaxial Co/Pd(111) system is motivated by the recent demonstration of a huge spin-orbit torque effect in polycrystalline Co/Pd multilayer nanowires. In spite of discovery of PMA in the Co/Pd superlattices as far back as the 1980s [7], the origin of PMA in the epitaxial Co/Pd(111) system is still under debate.

The occurrence of PMA in ferromagnetic/nonmagnetic superlattices was initially explained by the Néel theory [8]. Néel proposed that interface atoms reveal magnetic anisotropy unlike that of the bulk because of reduced symmetry at the interface. Several groups then investigated PMA in superlattices and particularly in the Co/Pd system by first-principles calculations. Daalderop *et al.* [9] pointed out that several factors play a key role in the emergence of PMA: the position of the Fermi energy close to the doubly degenerate state with a particular orbital number and strong hybridization between Co 3*d* states with a large exchange splitting but a small spin-orbit interaction and Pd 4*d* states with a small exchange splitting but a large spin-orbit interaction. Bruno *et al.* [10] showed that the energy of PMA in thin Co layers is related to anisotropy of the orbital moment of interface atoms. Due to large spin-orbit coupling in heavy metal and hybridization of electronic states of ferromagnetic and heavy metals, the anisotropy of the orbital moment gives rise to strong PMA in the interface layers.

PMA caused by modification of the electronic structure at the interface is usually referred to as interface magnetocrystalline anisotropy (IMA). Another possible mechanism of induction of PMA in Co/Pd superlattices is related to elastic strains due to a lattice mismatch between ferromagnetic and nonmagnetic metals. It is energetically unfavorable to accumulate elastic strains in the volume of the ferromagnetic film; hence, after attaining critical thickness, elastic strains relax by misfit dislocation formation. The region of the ferromagnetic film containing most of the elastic strains in systems with large lattice mismatch is rather thin and may be considered as an interface region. PMA caused by elastic strains in the ferromagnetic layers is named magneto-elastic anisotropy (MEA), which may be considered as volume or interface anisotropy because of the dependence on the thickness of the ferromagnetic film.

Usually, the aforementioned two mechanisms coexist with each other, and it is a challenge to measure the contribution of a particular mechanism to PMA. The structure of the interfaces should also be taken into account. Interfaces may be sharp or intermixed with surface alloy formation. The magnetic properties and magnetic anisotropy of the surface Co_xPd_{1-x} alloys are strongly different from the magnetic properties and anisotropy of pure Co films. PMA is induced in alloyed interface Co_xPd_{1-x} regions through the strain anisotropy of Co atoms [11,12]. A magnetostriction constant λ_{111} of the order of -1×10^{-4} was measured in Co_xPd_{1-x} alloyed films.

The roughness of interfaces may influence the energy of the induced PMA. The influence of the roughness may be considered from two viewpoints. On the one hand, introduction of the interface roughness reduces the negative energy of the shape anisotropy $-\mu_0 M_s^2/2$ of a perfectly flat film and enhances the PMA [10]. This mechanism is based on dipolar interaction and seems to be universal for all systems; however, the magnitude of the effect is not very large. On the other hand, a rough interface decreases the spin projected occupation number ratio of the magnetic quantum number and hence reduces the PMA [13]. Therefore, the influence of roughness on PMA is arguable. Nevertheless, experimental findings show a decrease of PMA with increasing interface roughness in the Co/Pd system [14,15].

Many papers have been devoted to investigation of PMA in epitaxial Pd/Co/Pd(111) trilayers and Co/Pd(111) superlattices. Some scientific groups consider that PMA in this system is predominately IMA [16–18]. Moreover, it

*Corresponding author: avdavydenko@gmail.com

was experimentally shown that interface anisotropy does not depend on the crystallographic orientation of the Co layers [19]. In other papers, PMA in a Co/Pd(111) system is related to stress and treated as MEA [20]. In some papers, PMA in Co/Pd(111) superlattices is explained by CoPd surface alloy formation [21]. However, in this case, both the magneto-elastic and magnetocrystalline anisotropies may contribute to PMA, because Co atoms located in the Pd environment have a modified electronic structure and simultaneously undergo stress. In spite of the abundance of experimental results, the origin of the PMA in a Co/Pd(111) system remains unclear. In the present paper, various possible contributions to the PMA in Pd/Co/Pd(111) trilayers are carefully analyzed and discussed. The influence of growth conditions and the structure of interfaces on the PMA is clarified. The asymmetry of the contribution to PMA from the bottom Co/Pd and the top Pd/Co interfaces is determined.

II. MODEL FOR CALCULATION OF PMA

A common phenomenological approach used to investigate the origin of PMA in a magnetic film is to introduce the effective magnetic anisotropy (EMA), K_{eff}, as the sum of the volume and surface magnetic anisotropies:

$$K_{\text{eff}} = K_v + \frac{K_s}{t_{\text{FM}}}, \tag{1}$$

where K_v and K_s are the summed energies of volume and surface anisotropies, respectively, and t_{FM} is the thickness of the magnetic film. K_v includes the shape anisotropy $K_{\text{shape}} = -\mu_0 M_s^2/2$ and volume magnetocrystalline anisotropy K_{MCA}. K_s contains the contribution of IMAs from the bottom and top interfaces caused by electronic effects, K_{s1} and K_{s2}, respectively.

To separate the surface K_s and volume K_v contributions to PMA, $K_{\text{eff}} \times t_{\text{FM}}(t_{\text{FM}})$ dependence is usually investigated:

$$K_{\text{eff}} \times t_{\text{FM}}(t_{\text{FM}}) = K_v \times t_{\text{FM}} + K_s = \left(-\frac{\mu_0 M_s^2}{2} + K_{\text{MCA}}\right) \times t_{\text{FM}} + K_{s1} + K_{s2}. \tag{2}$$

In the case of strained growth of a ferromagnetic film on a lattice-mismatched substrate, MEA must be taken into account. If the lattice mismatch between a substrate material and a film is not too large, growth initially takes place in the coherent regime characterized by full lattice registry. Strain in a magnetic film is constant in the coherent regime of growth. At a certain critical thickness, t_c, the energy of the elastic strains becomes larger than the energy necessary for misfit dislocation formation. Hence, beginning from the critical thickness, misfit dislocations develop and relax the elastic strain until the value of the lattice parameter of the film becomes equal to the volume value. Growth occurs in the incoherent regime after the critical thickness t_c.

It was shown by den Broeder *et al.* that separate interpretation of the MEA must be carried out in the regions of coherent and incoherent growth of a ferromagnetic layer [16]. MEA is considered to be of volume-type $K_{v,\text{MEA}}$ in the coherent regime and to be of surface-type $K_{s,\text{MEA}}$ in the incoherent regime. Crossover between these two regimes is revealed as a kink at t_c in the Co thickness dependence of $K_{\text{eff}} \times t_{\text{FM}}$. The analytical expressions of $K_{v,\text{MEA}}$ and $K_{s,\text{MEA}}$ were derived in the special case of ferromagnetic/nonmagnetic multilayers.

In this paper, we propose a model for the numerical calculation of MEA based on the experimentally measured elastic strains in ferromagnetic films using reflection high-energy electron diffraction (RHEED) and approve it on a Pd/Co/Pd(111) epitaxial system. MEA for an epitaxial film with (111) orientation on a (111) substrate is written as [22]

$$K_{\text{MEA}} = -\tfrac{3}{2}\lambda_{111}\bar{\sigma} = -\tfrac{3}{2}\lambda_{111}\text{E}\bar{\varepsilon}, \tag{3}$$

where $\bar{\sigma}$ is the average stress, $\bar{\varepsilon}$ is the average strain in the film, E is the elastic modulus of ferromagnetic material, and λ_{111} is the saturation magnetostriction constant along the $\langle 111 \rangle$ direction. In the case of epitaxial growth, strain in a certain layer of the magnetic film is defined as a lattice mismatch between the lattice parameter of this layer and the volume lattice parameter:

$$\varepsilon(t_{\text{FM}}) = \frac{a(t_{\text{FM}}) - a_0}{a_0}, \tag{4}$$

where $a(t_{\text{FM}})$ is the lattice parameter of the specific layer, which depends on the thickness of the film under this layer and which can be measured by RHEED, and a_0 is the volume lattice parameter of the magnetic material. The average strain in the film may be calculated using the experimentally measured thickness dependence of the strain $e(t_{\text{FM}})$

$$\bar{\varepsilon} = \frac{\int_0^{t_{\text{FM}}} \varepsilon(t_{\text{FM}}) dt_{\text{FM}}}{t_{\text{FM}}}. \tag{5}$$

Substitution of (5) into (3) gives the averaged MEA

$$K_{\text{MEA}} = \frac{-\tfrac{3}{2}\lambda_{111}\text{E}\int_0^{t_{\text{FM}}} \varepsilon(t_{\text{FM}}) dt_{\text{FM}}}{t_{\text{FM}}}. \tag{6}$$

Taking into account the different contributions to K_v and K_s and Eq. (6), the $K_{\text{eff}} \times t_{\text{FM}}(t_{\text{FM}})$ dependence is defined as

$$K_{\text{eff}} \times t_{\text{FM}} = \left(-\frac{\mu_0 M_s^2}{2} + K_{\text{MCA}}\right) \times t_{\text{FM}} - \frac{3}{2}\lambda_{111}\text{E}\int_0^{t_{\text{FM}}} \times \varepsilon(t_{\text{FM}}) dt_{\text{FM}} + K_{s1} + K_{s2}. \tag{7}$$

An example of the $K_{\text{eff}} \times t_{\text{FM}}(t_{\text{FM}})$ curve calculated by Eq. (7) using positive K_{s1} and K_{s2} values, negative shape anisotropy, and the profile of strain relaxation, which is inversely proportional to the thickness of the magnetic film after t_c, the negative magnetostriction constant, and positive strains corresponding to the expanded magnetic layer is shown in Fig. 1.

The calculated curve agrees well with the schematic curve proposed by den Broeder *et al.*, demonstrating the necessary kink. Moreover, Eq. (6) takes into account the gradual relaxation of the strains, which provides a gradual transition from the volume-type MEA to the surface-type MEA.

Indeed, up to the critical thickness, t_c, the averaged strains do not depend on the Co thickness (coherent regime), and the MEA calculated by Eq. (6) remains constant: $K_{\text{MEA}}(t_{\text{FM}} < t_c) = K_{v,\text{MEA}} = -\tfrac{3}{2}\lambda_{111}\text{E}\varepsilon_0$, where ε_0 is the constant strain in the coherent regime of growth. MEA may be considered as volume anisotropy. If the magnetostriction constant is negative and the strain is positive (as in the case of growth of Co on

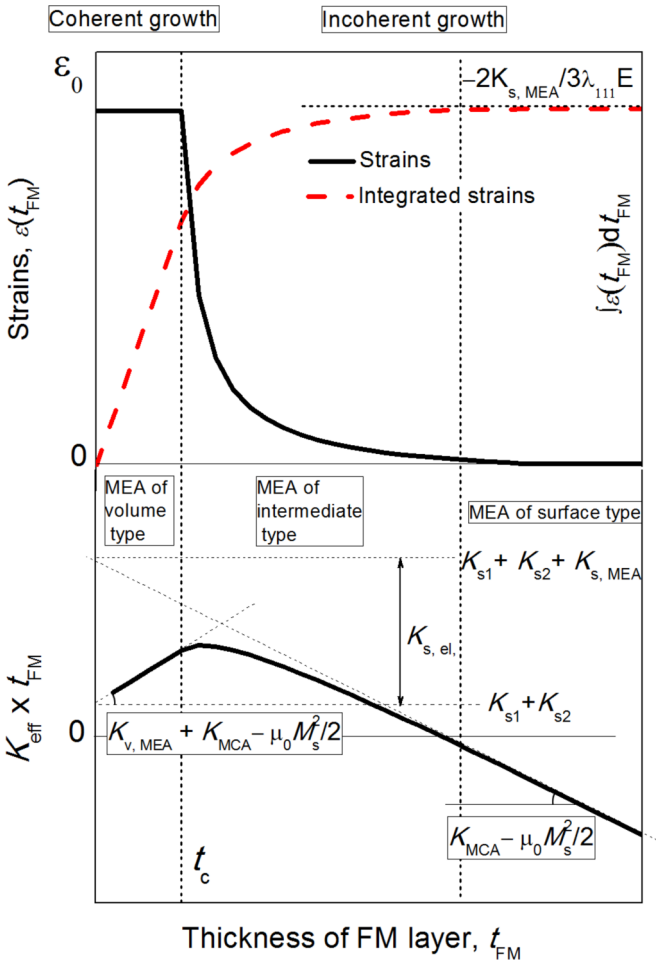

FIG. 1. Scheme of the dependencies of the strains $\varepsilon(t_{\mathrm{FM}})$, integrated strains $\int_0^{t_{\mathrm{FM}}} \varepsilon(t_{\mathrm{FM}})dt_{\mathrm{FM}}$, and $K_{\mathrm{eff}} \times t_{\mathrm{FM}}(t_{\mathrm{FM}})$ on the thickness of the magnetic layer.

Pd) up to the critical thickness, the integral $\int_0^{t_{\mathrm{FM}}} \varepsilon(t_{\mathrm{FM}})dt_{\mathrm{FM}}$ gives a positive constant slope in the thickness dependence $K_{\mathrm{eff}} \times t_{\mathrm{FM}}(t_{\mathrm{FM}})$.

After the critical thickness, the strains in the magnetic film begin to relax. Integrated strains, which are expressed by the integral $\int_0^{t_{\mathrm{FM}}} \varepsilon(t_{\mathrm{FM}})dt_{\mathrm{FM}}$ in Eq. (6), are less dependent on the thickness t_{FM} and gradually converge to a constant value $-\frac{2K_{s,\mathrm{MEA}}}{3\lambda_{111}\mathrm{E}}$. The volume contribution of the MEA progressively decreases, which reveals the scheme by the change in slope from positive to negative. In this intermediate-thickness interval, the MEA changes its behavior from the volume type to the surface type of anisotropy. Note that the position of t_c is not defined by the maximum of the $K_{\mathrm{eff}} \times t_{\mathrm{FM}}(t_{\mathrm{FM}})$ dependence, but it corresponds to the onset of the nonlinearity of the $K_{\mathrm{eff}} \times t_{\mathrm{FM}}(t_{\mathrm{FM}})$ curve after its linear behavior in the coherent regime.

If the total thickness of the magnetic film becomes much greater than the critical thickness, strains are almost fully relaxed, and the MEA contribution may be considered as a surface magnetic anisotropy contribution, $K_{\mathrm{MEA}}(t_{\mathrm{FM}} \gg t_c) = \frac{K_{s,\mathrm{MEA}}}{t_{\mathrm{FM}}}$. This thickness interval is characterized by a constant negative slope of the $K_{\mathrm{eff}} \times t_{\mathrm{FM}}(t_{\mathrm{FM}})$ dependence. Hence, for correct determination of $K_{s,\mathrm{MEA}}$, one needs to make sure that $K_{\mathrm{eff}} \times t_{\mathrm{FM}}(t_{\mathrm{FM}})$ reaches a constant slope after t_c. Otherwise, the measured value of $K_{s,\mathrm{MEA}}$, and hence the value of the sum of surface anisotropies $K_s = K_{s1} + K_{s2} + K_{s,\mathrm{MEA}}$, will be understated.

The observed behavior of MEA may be qualitatively described. When the total thickness of the magnetic film becomes sufficiently larger than the thickness of the strained volume of the film, then, with a good accuracy, it may be considered that strains in the film are not distributed in the volume but are concentrated only at the interface. Hence, MEA behaves like surface anisotropy in this case.

A change in the slope of an experimental $K_{\mathrm{eff}} \times t_{\mathrm{FM}}(t_{\mathrm{FM}})$ curve is often interpreted as the manifestation of the MEA, which is thickness dependent. However, this does not always hold. Theoretical investigations predict that the surface anisotropies K_{s1} and K_{s2} are not strictly localized at the interface but rather propagate in the bulk magnetic layers with attenuation [23]. The growth of magnetic layers generally occurs not by a layer-by-layer mechanism but rather via three-dimensional (3D) island formation. Hence, the interface will be fully completed only at the coverage at which the first magnetic layer coalesces (2–3 monolayers [ML]). In addition, intermixing may occur in the interface regions, and hence magnetic atoms in nonmagnetic proximity may be distributed over several layers. Therefore, K_{s1} and K_{s2} need to be considered as volume magnetic anisotropies if the thickness of the ferromagnetic film is only a few monolayers. Nevertheless, usually interface anisotropies are considered as constants that do not depend on the thickness of the magnetic film, and this assumption does not contradict experimental results. In most papers, the minimal thickness of the investigated films is 3 ML or more due to the limitation of experimental sensitivity [24–26]. This minimal thickness already includes the greatest part of the surface anisotropies because of rapid attenuation of the surface anisotropies in the bulk layers.

III. EXPERIMENT

The samples were evaporated in an Omicron ultrahigh-vacuum system, which consisted of a molecular beam epitaxy chamber and an analysis chamber interconnected with each other. We used Si(111) substrates misoriented towards [11–2] by 0.1°. Before loading into the chamber, Si(111) substrates were rinsed in isopropyl and distilled water. Then, the substrates were heated at 800 K by indirect heating for 12 h. Just before deposition, the substrates were flash-heated by direct current at 1500 K three times for 10 sec and slowly cooled down to 300 K. All the metals were evaporated from high-temperature effusion cells. In this work, we measured the thicknesses of the layers in monolayers (ML). One $\mathrm{ML_{Cu}}$ corresponds to the thickness of one ideal layer of Cu, which is equal to 2.09 Å, 1 $\mathrm{ML_{Co}}$ = 2.05 Å, and 1 $\mathrm{ML_{Pd}}$ = 2.25 Å. The growth rates of Cu, Co, and Pd were 4.3, 1.3, and 0.75 ML/min, respectively. The deposition rates were monitored by a quartz crystal microbalance, which was calibrated by means of RHEED. We detected the oscillations of the intensity of the specular beam reflection during the growth of Cu on Si(111), Co on Cu(10 ML)/Si(111), and Pd on Cu(10 ML)/Si(111). Then, we calculated the period of oscillations and compared it with data obtained from the quartz crystal microbalance.

The temperature of the substrates was 340 K during Cu and Pd deposition and 380 K during Co deposition. Changes in the temperature of the samples during deposition of different materials were caused by different radiative heating of the samples from the effusion cells. Epitaxial Pd/Co/Pd(111) trilayers were grown on a Cu(10 ML)/Si(111) surface. To define the origin of the PMA in this system, several series of samples were prepared with specified constant thicknesses of the bottom and top Pd layers and different thicknesses of the Co layer (2–25 ML). Investigated thicknesses of the bottom Pd layer were 5, 10, and 24 ML, and the thickness of the top Pd layer was 10 ML. A series of samples was prepared in which the bottom or top Pd layer was replaced by the Cu(10 ML) layer. Finally, the PMA was measured in Cu/Co/Cu(111) trilayered films. Consequently, the investigated series of trilayers with different Co thicknesses was as follows: Pd(10 ML)/Co/Pd(24 ML), Pd(10 ML)/Co/Pd(10 ML), Pd(10 ML)/Co/Pd(5 ML), Cu(10 ML)/Co/Pd(10 ML), Pd(10 ML)/Co/Cu(10 ML), and Cu(10 ML)/Co/Cu(10 ML).

In addition, a series of samples with structures of Pd(10 ML)/Co(4 ML)/Pd(0–68 ML)/Cu(10 ML)/Si(111) and Pd(0–36 ML)/Co(4 ML)/Pd(24 ML)/Cu(10 ML)/Si(111) was grown to distinguish the contributions to PMA from the bottom and top Co/Pd interfaces. The growth and topography of the Co layers on Pd/Cu/Si(111) were investigated *in situ* using a scanning tunnelling microscope (STM) manufactured by Omicron. STM images were obtained on the same sample by alternation of the deposition and scanning processes. The lattice period of the metal layers during growth and their structure were analyzed by means of RHEED (Staib Instruments). RHEED measurements were done simultaneously with deposition of the samples. Magnetic characterization of the samples was carried out using a vibrating sample magnetometer (VSM) manufactured by Lakeshore with applied magnetic fields of up to 27 kOe.

IV. RESULTS AND DISCUSSION

A. Growth processes and structure

1. Pd/Cu(10 ML) on Si(111)

A Cu(10 ML) buffer layer was formed on the Si(111) substrate to prevent intermixing of Pd and Si and to initiate epitaxial growth of face centered cubic (fcc) Pd(111). Cu(111) grows on Si(111) in layer-by-layer two-dimensional growth mode starting from coverage of 3 ML [27]. The epitaxial relationships defined from the RHEED patterns are Cu(111)‖Si(111) and $Cu_{[11-2]}$‖$Si_{[10-1]}$. The epitaxial relationships during growth of the subsequent Pd and Co layers remained unchanged. Growth of Pd on Cu(10 ML)/Si(111) was investigated in detail in our previous paper [28]. Pd(111) grows on Cu(10 ML)/Si(111) by 3D island growth mode from the beginning of growth. Up to a Pd thickness of 2.6 ML, the Pd film is the most disordered. Most of the strains in the Pd film relax in this stage. Surface alloying of Pd with Cu is possible at this stage of growth. In the thickness interval from 2.6 to 13 ML, the roughness of the Pd does not change significantly, and the Pd grows in a layer-by-layer–like mode. During the second stage, the lattice parameter of the Pd film gradually increases to the volume value. With increasing coverage after 13 ML, the lattice parameter does not change, but the roughness of the Pd films increases rapidly. Pd islands grow in height and lateral size. Pd grows in an fcc structure, which may be twinned [29].

2. Co on Pd/Cu(10 ML)/Si(111)

The growth of Co on Pd(t_{Pd1})/Cu(10 ML)/Si(111) surfaces was investigated at different thicknesses of Pd bottom layers: t_{Pd1} = 5, 10, 18, and 24 ML. Despite the large 9.6% lattice mismatch between Co and Pd, Co(111) grows on Pd(111) epitaxially with a high degree of crystal order. As deduced by RHEED, Co grows in a (111) orientation, repeating the epitaxial relationships of the bottom Pd(111) layer. Accurate determination of the Co structure, which may be hexagonal close packed (hcp) or fcc, cannot be performed using only RHEED; however, based on the analysis of magnetic properties, it is supposed that Co grows predominately in fcc structure. This conclusion is in agreement with literature data [30,31]. The dependencies of the RHEED intensity during growth of Co on Pd(5, 10, and 24 ML)/Cu(10 ML)/Si(111) surfaces are presented in Fig. 2(a). The dependencies are generally similar except for the position of the minima. The different coverages of Co at which minima are observed are related to the roughness of the Pd bottom layer. With increasing roughness of the Pd bottom layer, the coverage of Co at which the RHEED minimum is observed increases as well. The RHEED intensity falls rapidly to the minimum and then gradually increases almost to the initial values. In the case of deposition of Co on Pd(5 ML)/Cu/Si and Pd(10 ML)/Cu/Si surfaces, weak RHEED oscillations can be recognized after deposition of approximately 4.7 ML coverage of Co. The lattice parameter of Co during the deposition on the Pd(5, 10, and 24 ML)/Cu(10 ML)/Si and Cu(10 ML)/Si surfaces as a function of Co coverage is shown in Fig. 2(b). At the beginning of growth, the Co lattice parameter nearly coincides with the lattice parameter of the Pd underlayer, which means that Co interface layers are largely expanded. The lattice parameter of Co changes gradually, which indicates gradual strain relaxation. Strains in the interface Co layers increase with increasing thickness of the Pd underlayer. Note that a strain of 0.75% persists in the Co layer even at 25 ML coverage independent of the type of bottom surface.

To analyze the growth processes of Co, a comparison of the RHEED intensity and the lattice parameter dependencies with evolution of the RHEED patterns was carried out for the growth of Co on the Pd(24 ML)/Cu(10 ML)/Si(111) surface. The RHEED pattern from the Pd(24 ML)/Cu(10 ML)/Si(111) surface is shown in Fig. 2(c). Up to 1 ML, coverage of deposited Co does not influence the observed RHEED pattern much. A slight decrease of the specular beam intensity and shifting of the RHEED streaks are registered. The largest changes in the RHEED patterns occur after deposition of 1 to 4 ML of Co. In this thickness interval, most of the strains relax in the Co layer. The RHEED intensity falls to a minimum at Co coverage of 2.5 ML. At this coverage of Co, RHEED streaks are the most diffuse, and the intensity of the background is maximal [Fig. 2(d)]. After 2.5 ML of Co

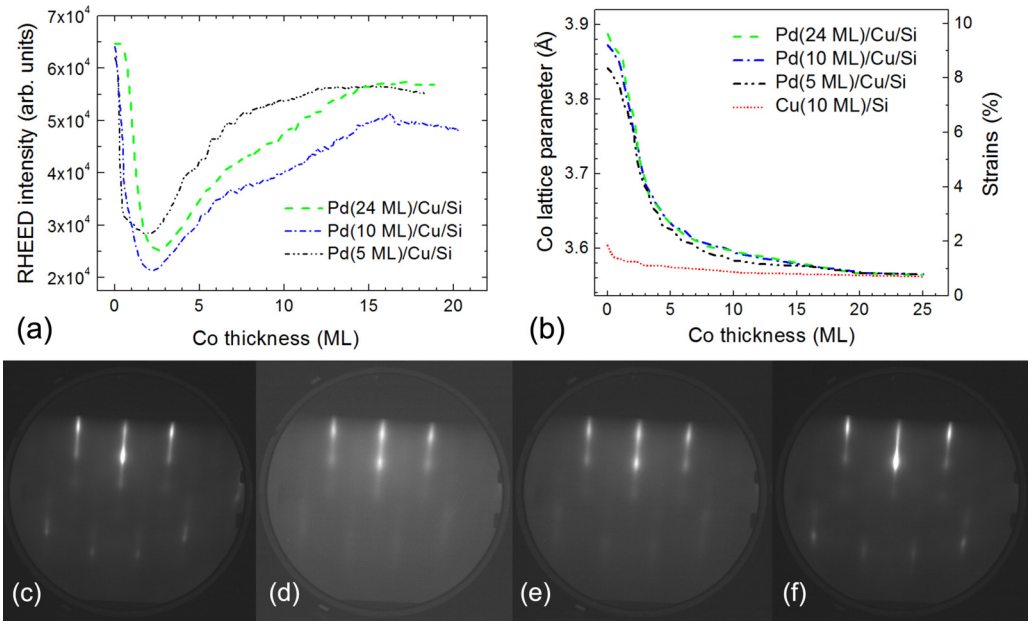

FIG. 2. Dependencies of (a) the RHEED specular beam intensity and (b) the Co lattice parameter and strains on the thickness of the Co layer deposited on Pd/Cu/Si(111) surfaces with different thicknesses of Pd bottom layers and on Cu/Si(111). RHEED patterns of (c) the Pd(24 ML)/Cu/Si surface and of the surface of Co layers deposited on Pd(24 ML)/Cu/Si(111) with thicknesses of (d) Co(2.5 ML), (e) Co(4 ML), and (f) Co(10 ML).

coverage, the intensity of the background gradually decreases, and the RHEED streaks become narrower [Figs. 2(e) and 2(f)].

Growth processes of Co on the Pd(18 ML)/Cu(10 ML)/Si(111) surface were investigated by STM. The Pd(18 ML)/Cu(10 ML)/Si(111) surface is rather rough [Fig. 3(a)]. The lower layers tend to coalesce, while the upper layers represent separate 3D islands with lateral sizes of 20–25 nm. The edges of the islands are not well faceted. A surface of Co(0.25 ML)/Pd(18 ML)/Cu/Si(111) is shown in Fig. 3(b). Co atoms mostly decorate the step edges of the Pd islands; hence, the edges of the islands become irregular and wavy. With deposition of 1 ML of Co, separate monolayer-height Co islands are nucleated [Fig. 3(c)]. The lateral sizes of the separate Co islands are 2–5 nm. With further growth, separate Co islands coalesce, forming large pure Co islands [Fig. 3(d)]. A small number of monolayer-height islands is still observed. At Co coverage of 10 ML, Co islands have a well-defined hexagonal shape and lateral sizes comparable with the sizes of the initial Pd islands [Fig. 3(e)]. However, the root-mean-square (RMS) roughness of the Co(10 ML) surface is lower than that of the Pd bottom layer [Fig. 3(f)]. From this observation, it may be concluded that Co smooths the rough surface of the Pd bottom layer. Coalescence of separate Co islands is expected at approximately 2–3 ML of Co coverage. This growth mode is favorable for the preparation of epitaxial Co/Pd multilayered films, since Co will smooth the increasing roughness of Pd interlayers.

Based on the literature data, it may be concluded that the growth processes of Co on a Pd/Cu/Si(111) surface are similar to the growth processes of Co on a Pd(111) single crystal surface. Wasniowska *et al.* [32] investigated the growth processes of Co on a Pd(111) single crystal by STM. They investigated 3D growth of Co at 300 and 550 K and found that the shape of the Co islands was hexagonal during growth at 300 K and trigonal at 550 K. Evolution of the Co lattice parameter during growth on Pd(111) at 300 K was investigated by RHEED [33]. It was shown that Co grows with its natural lattice parameter from the beginning of growth, which evidences the incoherent growth of Co at room temperature. Similar results were obtained by Boukari *et al.* [34]. It was also found that at 370 K, the mechanism of strain relaxation changed completely. At elevated temperature, strains in the Co film relax gradually, and a residual strain of 1.5% remains in the Co film even at 28 ML coverage. Our results corroborate gradual strain relaxation in Co during growth on Pd(111) at 380 K.

Brief conclusions may be drawn based on the aforementioned results. Co does not grow pseudomorphically on the Pd/Cu/Si surface. Strain relaxation in Co occurs from the beginning of growth, but it does so gradually if the temperature of the substrate is 380 K. The increasing background intensity and width of the RHEED streaks in the initial stages of Co growth signify the high density of defects (misfit dislocations [32]) and maximal disorder. Most of the strains relax up to 4 ML of deposited Co. Gradual strain relaxation and structural improvement occur with further deposition of Co coverage of more than 4 ML.

3. Pd(111) on Co/Pd(24 ML)/Cu(10 ML)/Si(111)

The top Pd layer grows on the Co(111) surface, conserving epitaxial relationships of the bottom Co layers. The top Pd layer continues 3D island growth. However, the mechanism of strain relaxation during growth of the top Pd layer on Co differs significantly from the mechanism of strain relaxation in Pd growing on the Cu buffer layer. We observed separate streaks from Co and Pd even at Pd coverages of 0.1 ML deposited on the Co(20 ML)/Pd(24 ML)/Cu/Si(111) surface.

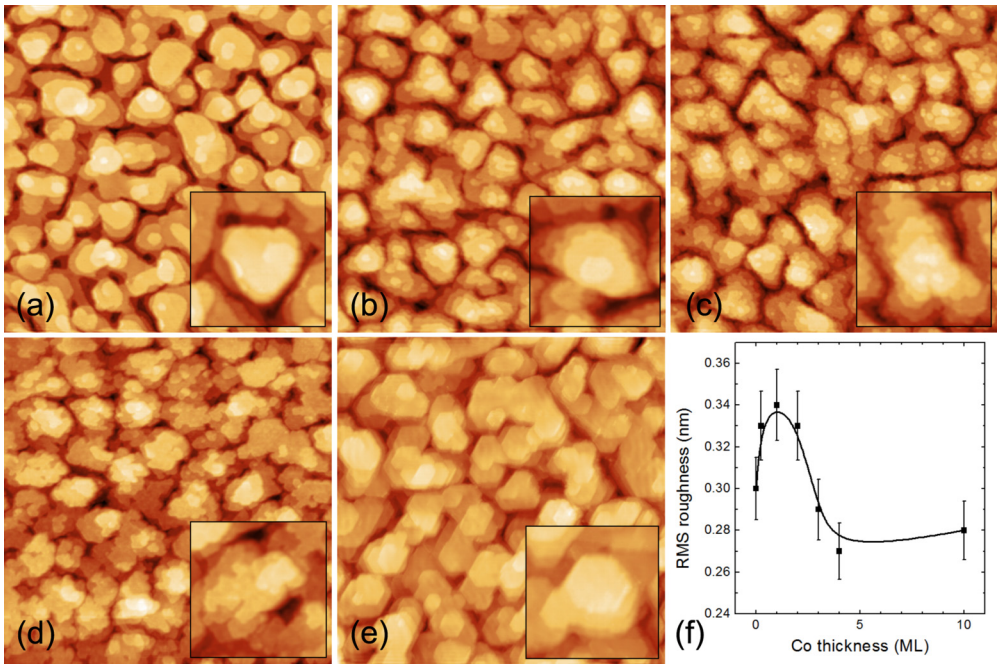

FIG. 3. 200 nm × 200 nm STM images of (a) Pd(18 ML)/Cu/Si(111) surface and Co layers deposited on Pd(18 ML)/Cu/Si(111) surfaces with thicknesses of (b) 0.25 ML, (c) 1 ML, (d) 4 ML, and (e) 10 ML. Scaled-up 40 nm × 40 nm areas with separate islands are shown in the insets. (f) RMS roughness as a function of the Co layer thickness; the solid line is the B-spline interpolation of the experimental points.

Observation of the separate RHEED streaks from Pd and Co indicates the presence of isolated Pd islands with the natural Pd lattice parameter on the Co surface. The intensity of the RHEED streaks from Co decreases with further deposition of Pd, while the intensity of the RHEED streaks from Pd increases. Similar double-streaked RHEED patterns were observed during growth of Pd on Co layers with smaller thicknesses; however, precise separation of the signals from Co and Pd is difficult in this case because of broadening of the RHEED streaks from thin Co layers. The RHEED pattern of the Pd(0.6 ML)/Co(20 ML)/Pd(24 ML)/Cu/Si(111) surface is presented in Fig. 4(a). At this Pd coverage, the intensities of the streaks from Pd and Co are nearly equal to each other. We extracted RHEED intensity profiles across the streaks from Co and Pd separately by using multiple fitting of Lorentzian-type peaks [shown in the inset of Fig. 4(a)].

A dependence of the Co and Pd lattice parameters on the thickness of the Pd overlayer is shown in Fig. 4(b). The Co lattice parameter of the top Co layer and hence the strains increase with increasing Pd coverage. The lattice parameter of Pd increases stepwise in the early stages of growth, then decreases up to 1.6 ML coverage, and finally increases again. Strains in the interface Co layer cannot be measured directly by RHEED if the thickness of the Pd overlayers is more than 1.2 ML, because of the disappearance of the signal from Co. However, we suppose that the strains in Co increase linearly up to 1.6 ML of Pd coverage, owing to the initial Pd contraction, which cancels out Co expansion. With subsequent deposition of Pd of more than 1.6 ML, strains in Co do not increase and remain at nearly 1.5% in the interface Co layer [shown in the inset of Fig. 4(b)]. If Pd and Co are deposited on the Pd(24 ML)/Cu(10 ML)/Si(111) surface, strains in the top Co interface layers (1.5%) are much lower than the strains in the bottom Co interface layers (9.6%).

B. Perpendicular magnetic anisotropy investigation

1. Method of magnetic anisotropy measurement and study of saturation magnetization

The effective anisotropy K_{eff} at a certain Co thickness is defined as the area between the magnetization curves measured perpendicular and parallel to the plane of the films, $M_{\perp}$ and $M_{\parallel}$, divided by the total volume of magnetic layers:

$$K_{\text{eff}} = \frac{1}{V}\int_0^{H_{\text{sat}}} (M_{\perp} - M_{||})dH. \tag{8}$$

For correct determination of EMA, the dependencies of the saturation magnetization on the Co thickness must be taken into account. Also, the dependence of the saturation magnetization on the thickness of the Co layer in the trilayered samples gives information about the sharpness of the interfaces. Intermixing of Co with Cu at the interfaces [35] may lead to the formation of magnetic dead layers that decrease the effective magnetization of the trilayered samples containing the Co/Cu interface. The dependence of the magnetic moment of the Cu(10 ML)/Co/Cu(10 ML) film normalized to the unit area on the Co thickness, taking into account magnetic dead layers, is expressed as

$$\frac{m}{S} = M_{\text{sat,Co}} t_{\text{FM}} = M_{\text{sat,Co}}(t_{\text{Co}} - t_{\text{CoCu}}), \tag{9}$$

where m is the magnetic moment of the sample measured by VSM, S is the surface of the sample, $M_{\text{sat,Co}}$ is the saturation magnetization of Co, t_{m} is the thickness of the

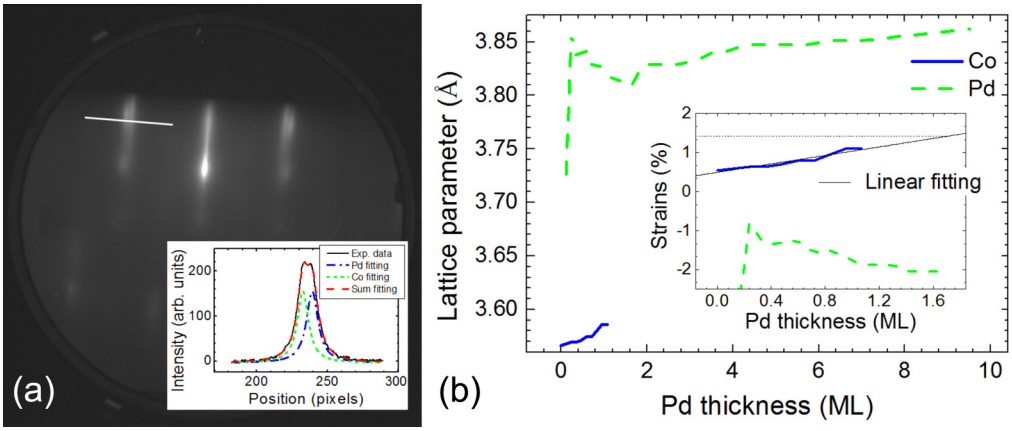

FIG. 4. (a) RHEED pattern of Pd(0.6 ML)/Co(20 ML)/Pd(24 ML)/Cu/Si(111) surface; the RHEED intensity profile with fitting is shown in the inset of Fig. 4(a). (b) The dependence of the lattice parameters of Co and Pd on the thickness of Pd overlayers deposited on the Co(20 ML)/Pd(24 ML)/Cu(10 ML)/Si(111) surface; strains in Co and Pd as a function of Pd thickness are shown in the inset of the Fig. 4(b).

magnetic layer, t_{Co} is the thickness of the deposited Co film, and t_{CoCu} is the total thickness of the bottom and top magnetic dead layers. Fitting of the experimental data for Cu/Co/Cu films by Eq. (9) gives $t_{CoCu} = 0.9 \pm 0.1$ ML and $M_{sat} = 1.44 \times 10^6$ A/m, which is close to the bulk value of the saturation magnetization for Co [Fig. 5(a)]. Reduction of the magnetic moment in ultrathin Co films can be explained not only by intermixing of Co with Cu, but due to the reduced Co magnetic moment in Co/Cu(111) interfacial layers. However, calculations show that the magnitude of the reduction is less than 5% in each Co interfacial layer [36]. In Fig. 5(b), we present the saturation magnetization of Cu/Co/Cu trilayers defined by Eq. (9) with and without taking into account the magnetic dead layers. The almost double reduction of the saturation magnetization in ultrathin Co layers cannot be explained only by the lowered magnetization of interfacial layers. Evidently, dead layers have to be considered. Indeed, calculation of the saturation magnetization with magnetic dead layers gives values close to the bulk value of Co saturation magnetization. It is worth noting that the thickness of the magnetic dead layers defined by fitting $m(t_{Co})/S$ dependence may include a contribution from reduced magnetization of interfacial Co layers. Hence, $t_{CoCu} = 0.9$ ML is the upper limit of the thickness of magnetic dead layers.

Substitution of Pd with Cu leads to polarization of the interface Pd atoms and enhancement of the magnetic moment of Co due to the magnetic proximity effect in Pd/Co/Pd films [37]. Equation (9) is modified in the case of Pd/Co/Pd trilayers as

$$\frac{m}{S} = M_{sat,av} t_m = M_{sat,Co} t_{Co} + M_{sat,Pd} t_{Pdpol}, \qquad (10)$$

where $M_{sat,av}$, $M_{sat,Co}$, and $M_{sat,Pd}$ are the saturation magnetizations of the whole magnetic volume, Co, and polarized Pd, respectively; t_m, t_{Co}, and t_{Pdpol} are the thicknesses of all the magnetic layers, the deposited Co layer, and the polarized Pd layers, respectively. Interception of the $m(t_{Co})/S$ dependence with the y axis gives a positive sum magnetic moment per unit area, $M_{sat,Pd} t_{Pdpol} = 6.3 \times 10^{-5}$ A, induced in the Pd interface layers. Using the value of the saturation magnetization of Pd $M_{sat,Pd} = 3.1 \times 10^5$ A/m [38], the effective thickness of two polarized Pd layers is calculated as $t_{Pdpol} = 0.2$ nm $= 0.9$ ML$_{Pd}$. The slope of the $m(t_{Co})/S$ dependence in Pd/Co/Pd samples corresponds to the saturation magnetization of $M_{sat,Co} = 1.52 \times 10^6$ A/m. This value is slightly higher than the bulk value of the Co saturation magnetization, 1.42×10^6 A/m, due to enhancement of the magnetic moment of Co. An influence of the polarized Pd layers is revealed in the thickness dependence of the saturation magnetization

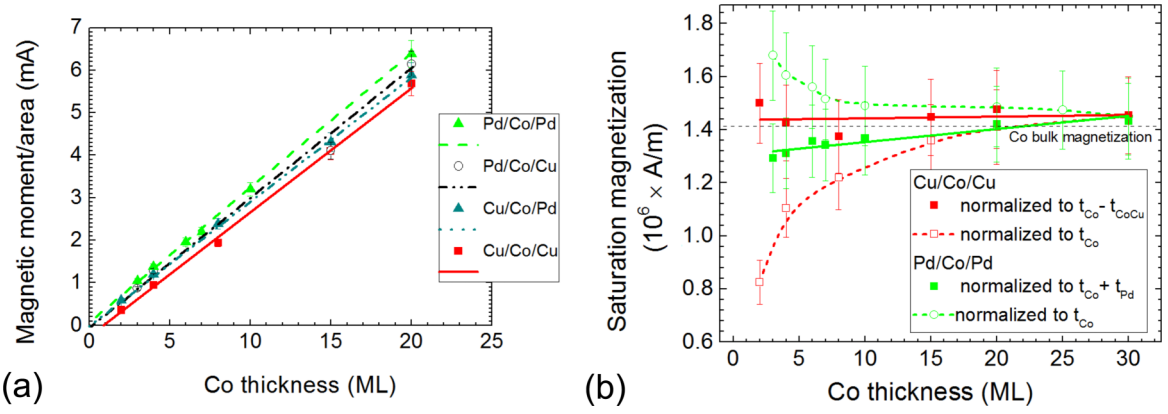

FIG. 5. The dependencies of (a) the magnetic moment per unit area in Pd/Co/Pd, Pd/Co/Cu, Cu/Co/Pd, and Cu/Co/Cu films and (b) the saturation magnetization on the Co thickness in Pd/Co/Pd and Cu/Co/Cu trilayers.

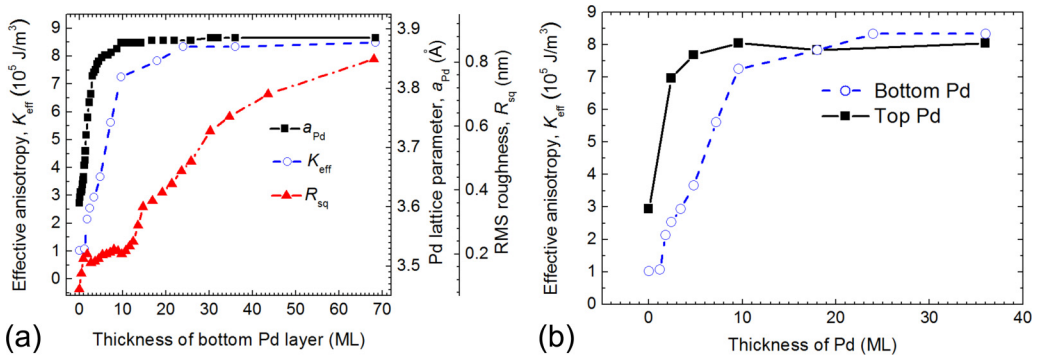

FIG. 6. (a) The dependencies of the energy of EMA, Pd lattice parameter, and RMS roughness of the bottom Pd_1 layer on the thickness of the Pd_1 layer in Pd_2(10 ML)/Co(4 ML)/Pd_1(0−68 ML) trilayers. (b) The dependencies of the energy of EMA on the thickness of the Pd bottom and top layers in the series of trilayered samples Pd_2(10 ML)/Co(4 ML)/Pd_1(0−68 ML) and Pd_2(0−36 ML)/Co(4 ML)/Pd_1(24 ML), respectively.

normalized to t_{Co} without addition of Pd polarized layers [Fig. 5(b)]. The magnetization of ultrathin Pd/Co/Pd trilayers is significantly higher than the bulk value. However, calculation of the average saturation magnetization using Eq. (10), and taking into account the Pd polarized layers, gives values close to the bulk value of Co saturation magnetization. A slight reduction of the saturation magnetization in the low-Co-thickness regime can be related to a decrease in the thickness of Pd polarized layers in the ultrathin-Co-thickness regime.

A slightly higher magnetic moment is observed in the Pd/Co/Cu samples than in the Cu/Co/Pd samples. Fitting of the experimental data for Cu/Co/Pd and Pd/Co/Cu samples in Fig. 5(a) gives values of Co saturation magnetization of 1.42 and 1.46 × 10^6 A/m, respectively. The average magnetization for mixed Pd/Co/Cu and Cu/Co/Pd trilayers cannot be calculated because the thicknesses of the dead and polarized layers of the detached bottom or top interfaces are not known. However, based on the results for Cu/Co/Cu and Pd/Co/Pd trilayers, it may be concluded that the bulk value of the Co saturation magnetization may be used in the calculation of the PMA energy in all series of samples with good accuracy.

2. *PMA as a function of thickness of the bottom* Pd_1 *and the top* Pd_2 *layers*

Since the top Pd_2/Co and bottom Co/Pd_1 interfaces have different strains, unequal contributions to the PMA from the top Pd_2/Co and bottom Co/Pd_1 interfaces are expected. To elucidate this issue, PMA was measured in the Pd_2/Co(4 ML)/Pd_1/Cu(10 ML)/Si(111) film as a function of bottom and top Pd layers. Two series of samples were investigated: Pd_2(10 ML)/Co(4 ML)/Pd_1(0 − 68 ML)/Cu(10 ML)/Si(11) and Pd_2(0 − 36 ML)/Co(4 ML)/Pd_1(24 ML)/Cu(10 ML)/Si(111). In the latter case, a Cu(10 ML) cap layer was deposited if the thickness of the Pd_2 top layer was less than 4 ML.

The dependence of the energy of EMA on the thickness of the Pd_1 layer in the first series of samples is shown in Fig. 6(a). Data for the Pd_1 lattice parameter and RMS roughness of the Pd_1 layer are taken from our previous paper for comparison [28]. Evidently, PMA does not depend on the roughness of the bottom interface. While the roughness remains almost constant, PMA strongly increases in the thickness interval of Pd from 2 to 10 ML, and vice versa—while the roughness increases considerably with the deposition of more than 10 ML of Pd, the PMA increases only slightly. The value of the Pd_1 lattice parameter in the Co/Pd_1 interface should strongly influence the magneto-elastic anisotropy. The general behaviors of the Pd_1 lattice parameter and the EMA are correlated, but significant differences are notable. The EMA remains constant up to 1.2 ML for the deposited Pd_1 bottom layer, while the Pd_1 lattice parameter increases from the beginning of Pd growth. This could be the sign of intermixing of Pd with Cu during epitaxial growth of Pd(111) on Cu(111) at near room temperatures. Such a possibility has been considered in a variety of papers [29,39,40]. This effect also indicates a large sensitivity of PMA to the chemical composition of the Co/Pd_1 interface. With further deposition of Pd, both the EMA and the Pd_1 lattice parameter increase; however, the Pd_1 lattice parameter begins to saturate after the deposition of 4 ML, while saturation of PMA begins only from 10 ML of Pd coverage.

Quantitative analysis of the contributions from the bottom and top Co/Pd interfaces was performed. The dependencies of the EMA on the thickness of the bottom Pd_1 layer in the first series of samples and the top Pd_2 layer in the second series are presented in Fig. 6(b). The different behaviors of the dependencies are evident. PMA is completely saturated only after deposition of 24 ML of the bottom Pd_1 layer and increases gradually with increasing thickness of the Pd_1 layer. However, PMA is already saturated at 5 ML of the Pd_2 top layer in the second series of samples. While the gradual rise of the PMA on the thickness of the bottom Pd_1 layer may be related to strains in the Co film and in the bottom Co/Pd_1 interface, the abrupt increase of PMA with the increasing thickness of the top Pd_2 layer is explained by the major contribution to PMA from the electronic structure of the top Pd_2/Co interface rather than from the volume strains in the Co film induced by the top Pd_2 layer. This preliminary consideration is confirmed by the asymmetry of the contributions from the top and bottom Pd interfaces. If the bottom and top Co/Cu interfaces contribute equally to PMA, insertion of the Pd_1 layer increases the PMA by 7 × 10^5 J/m^3, while insertion of the Pd_2 layer increases the PMA by only 5 × 10^5 J/m^3. In the following section, these quantitative results will be discussed more thoroughly.

3. *Perpendicular magnetic anisotropy as a function of Co layer thickness*

An analysis of the dependence of EMA on the thickness of the Co layer makes it possible to separate the energies of the surface and volume magnetic anisotropies. MEA may be calculated by Eq. (6) using the distribution of the strains in the magnetic film measured by RHEED [Fig. 1(b)]. However, two assumptions must be taken into account. First, RHEED obtains a signal not only from the topmost layer, but also from several top layers, depending on the angle of incidence and energy of electrons. We operated with a 15 keV electron beam. The penetration depth of the electrons was estimated by decaying the signal from Co with deposition of the Pd_2 layer on top of it. Deposition of only 1 ML of Pd led to a sixfold decrease of the RHEED signal from Co. Hence, it may be considered, with good accuracy, that the RHEED signal is captured only from the top layer in this work. Second, RHEED measures the lattice parameter of the top layer of the film during its growth. So, after formation of other layers on top of the investigated layer, the lattice parameter of the inner layer may change. We supposed that relaxation of the whole structure after completion of its growth is not significant.

EMA was measured in $Pd_2/Co/Pd_1$ trilayers with different thicknesses of the Co layer. The chosen thicknesses of the Pd_1 layer were 5, 10, and 24 ML, while the thickness of the Pd_2 layer was 10 ML. For the best reliability, EMA was measured in the series of samples with Pd substituted with Cu at the bottom or top interfaces in $Pd_2(10\,\text{ML})/Co/Cu_1(10\,\text{ML})$, $Cu_2(10\,\text{ML})/Co/Pd_1(10\,\text{ML})$, and $Cu_2(10\,\text{ML})/Co/Cu_1(10\,\text{ML})$ samples. EMA at all Co thicknesses was calculated using the bulk value of the Co saturation magnetization, $M_{\text{sat}} = 1420 \times 10^3$ A/m. The Co thickness dependencies $K_{\text{eff}} \times t_{\text{Co}}$ are shown in Fig. 7 for all the investigated series of samples. The experimentally measured values of EMA multiplied by the Co thickness were fitted by Eq. (7), where the elastic modulus for Co was taken as $E = 2.1 \times 10^{11}\,\text{N/m}^2$, and the magnetostriction constant was taken as $\lambda_{111} = -4.5 \times 10^{-5}$. The chosen value of λ_{111} is best for fitting and is relatively close to the experimentally measured value of the magnetostriction constant in fcc Co of -7×10^{-5} [41]. The fitting parameters for each series of samples are the volume magnetocrystalline anisotropy K_{MCA} and the IMAs caused by electronic effects at the bottom and top interfaces, K_{s1} and K_{s2}.

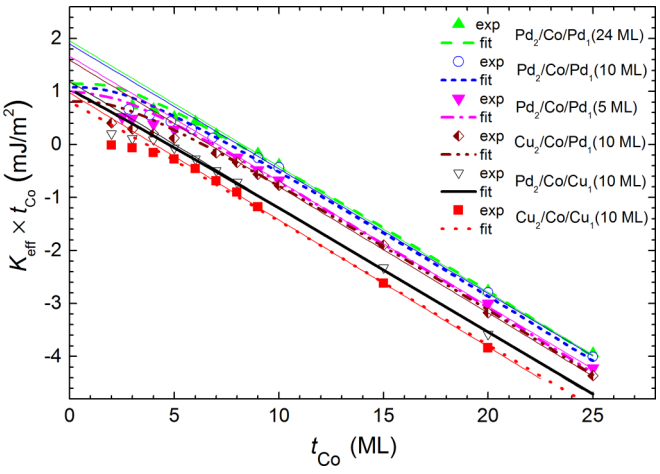

FIG. 7. Co thickness dependencies of $K_{\text{eff}} \times t_{\text{Co}}$ for different series of samples.

It is clearly seen that none of the fitted curves is in accordance with the experimental points at Co coverages of less than 5 ML. We suppose that, at these low Co coverages, IMAs cannot not be considered as constant values and begin to depend on the Co thickness due to the reasons described in Sec. II.

It appeared that K_{MCA} should be taken as zero to achieve the best fitting in all of the series of samples. All of the Co thickness dependencies have the same linear slope of $-1.16\,\text{MJ/m}^3$ after a Co thickness of 15 ML. The slope of the $K_{\text{eff}} \times t_{\text{Co}}(t_{\text{Co}})$ dependence after a Co thickness of 15 ML corresponds to the sum of the volume types of the anisotropies: shape, magnetocrystalline, and volume magneto-elastic. The shape anisotropy for Co is $K_{\text{shape}} = -\mu_0 M_s^2/2 = -1.27\,\text{MJ/m}^3$. At Co coverages of more than 15 ML, some residual strain still remains in all of the series of samples. This residual strain is not strongly dependent on further increase of the Co thickness and may be averaged to the value of $\varepsilon_{\text{res}} \cong 0.9\%$. Residual strain should contribute to the residual volume magnetic anisotropy, $K_{v,\text{MEAres}} = -\frac{3}{2}\lambda_{111} E \varepsilon_{\text{res}} = 0.13\,\text{MJ/m}^3$. So, the observed slope is approximately the sum of only the shape and the magneto-elastic anisotropies. The magnetocrystalline anisotropy seems to be negligible, which indicates that Co grows predominately in fcc structure on both Cu and Pd surfaces in the initial stages of growth.

Interception of the linear part of each curve with the y axis gives an experimentally measured total surface anisotropy, $K_{s,\text{exp}}$, which is the sum of the bottom and top IMAs and the surface anisotropy of magneto-elastic origin, K_{s1}, K_{s2}, and $K_{s,\text{MEA}}$, respectively.

$$K_{s,\text{exp}} = K_{s1} + K_{s2} + K_{s,\text{MEA}}. \tag{11}$$

Since there are six series of samples, we have a system of six equations with six unknown parameters: $K_{s1,\text{Cu}}$, $K_{s2,\text{Cu}}$, $K_{s1,\text{Pd(5 ML)}}$, $K_{s1,\text{Pd(10 ML)}}$, $K_{s1,\text{Pd(24 ML)}}$, and $K_{s2,\text{Pd(10 ML)}}$.

Fitting gives the MEA contribution, $K_{s,\text{MEA}}$, in each series of samples. Unfortunately, this system of equations could not be unambiguously solved. An accurate determination of the IMA at one surface of the Co layer is possible only when the IMA at the other surface is zero. To solve this system, it was assumed that the bottom and top IMAs in the Cu/Co/Cu system were equal to each other, $K_{s,\text{Cu1}} = K_{s,\text{Cu2}}$, and that the surface anisotropy from one side of the Co layer did not depend on the type of interface on the other side of the Co layer: $K_{s1,\text{Cu/Co/Cu}} = K_{s1,\text{Pd/Co/Cu}}$, $K_{s2,\text{Cu/Co/Cu}} = K_{s2,\text{Cu/Co/Pd}}$, $K_{s2,\text{Pd/Co/Cu}} = K_{s2,\text{Pd/Co/Pd}}$. In this case, the system of equations is completely solved, and the results are given in Table I. The results obtained from the six series of samples are quite well correlated with each other, signifying the reliability of the fitting.

A point that needs to be discussed is the multiplicity of the determined parameters depending on certain assumptions. The first problem is related to the value of the magnetostriction constant used, λ_{111}. We did not find any papers in which the magnetostriction constant of fcc Co λ_{111} was explicitly

TABLE I. Surface anisotropies in different types of systems, deduced from the fitting results.

Type of system	$K_{s,\mathrm{exp}}$	$K_{s,\mathrm{MEA}}$	K_{s1}	$K_{s1}+K_{s,\mathrm{MEA}}$	K_{s2}
			($\mathrm{mJ/m^2}$)		
$Cu_2/Co/Cu_1$	0.96	0.16	0.4	0.56	0.4
$Pd_2/Co/Cu_1$	1.2	0.16	0.4	0.56	0.64
$Cu_2/Co/Pd_1$(10 ML)	1.62	0.8	0.42	1.22	0.4
$Pd_2/Co/Pd_1$(5 ML)	1.67	0.67	0.36	1.03	0.64
$Pd_2/Co/Pd_1$(10 ML)	1.89	0.81	0.44	1.25	0.64
$Pd_2/Co/Pd_1$(24 ML)	1.95	0.82	0.49	1.31	0.64

determined. The value $\lambda_{111} = -7 \times 10^{-5}$ was measured in CoPd alloy films for extrapolation towards a 100% Co content [41]. Hence, some varying of the magnetostriction constant is feasible. In the present work, setting $|\lambda_{111}|$ higher than 4.5×10^{-5} does not allow the necessary slope of the $K_{\mathrm{eff}} \times t_{\mathrm{Co}}(t_{\mathrm{Co}})$ dependencies to be obtained. Setting $|\lambda_{111}|$ lower than 4.5×10^{-5} strongly decreases the contribution of MEA. In this case, the dependence of K_{s1} on the thickness of the Pd_1 bottom layer becomes stronger, which is unlikely.

The second question is related to the assumption that the bottom and top IMAs in the $Cu_2/Co/Cu_1$ system are equal to each other, $K_{s,\mathrm{Cu1}} = K_{s,\mathrm{Cu2}}$. Nonfulfillment of this assumption in the final analysis influences only the relation of $K_{s,\mathrm{Pd1}}$ and $K_{s,\mathrm{Pd2}}$. Asymmetry of the surface anisotropies in Cu/Co/Cu trilayers does not affect the values of calculated MEA and its contribution to the total PMA.

Analysis of the results shows that PMA in the Cu/Co/Cu system has a predominately electronic but not magneto-elastic origin. PMA in Cu/Co/Cu superlattices was investigated by Lee *et al.* [42]. They found similar EMA and a similar strain distribution in Co layers measured by x-ray diffraction. PMA in that system was explained predominately by the contribution of MEA. They fitted experimental data using the value of the magnetostriction constant multiplied by the Young's modulus $-3/2\lambda_s \mathrm{E} = -5.3 \times 10^7\ \mathrm{J/m^3}$. The latter value is almost four times higher than that used in the present paper. We tried to increase the magnetostriction constant in our fitting but did not obtain any appropriate results for either the Cu/Co/Cu or the Pd/Co/Pd series of samples. It is worth noting that the model for calculation of the magneto-elastic anisotropy in the work of Lee *et al.* does not include averaging of the strains over all the magnetic layers.

In Pd/Co/Pd trilayers, the MEA contribution to PMA may be comparable with the summed contribution to PMA from the bottom and top IMAs. $K_{s,\mathrm{MEA}} = 0.82\ \mathrm{mJ/m^2}$ in the Pd_2(10 ML)/Co($t_{\mathrm{Co}} > 15$ ML)/Pd_1(24 ML) trilayers, while $K_{s1} + K_{s2} = 1.13\ \mathrm{mJ/m^2}$ (see Table I). This case occurs only when the surface MEA, $K_{s,\mathrm{MEA}}$, is integrated over a strained film of large thickness, which includes most of the strains. Films with such large thickness have in-plane magnetic anisotropy and are inapplicable in practice. In thin Pd/Co/Pd films with a Co thickness of several monolayers, the MEA contribution will be lower due to the smaller number of strained layers included in the integration. When the strain distribution in the magnetic film is known, the MEA contribution to the total PMA may be easily calculated by Eq. (6) for a certain thickness of magnetic film and even compared with the IMA contribution. In the Pd_2(10 ML)/Co(4 ML)/Pd_1(24 ML) film, $K_{v,\mathrm{MEA}} = 0.85\ \mathrm{MJ/m^3}$, while $K_{s,\mathrm{IMA}}/t_{\mathrm{Co}} = (K_{s1} + K_{s2})/t_{\mathrm{Co}} = 1.4\ \mathrm{MJ/m^3}$.

The IMA from the top Pd_2/Co interface, $K_{s2} = 0.64\ \mathrm{mJ/m^2}$, is slightly larger than the IMA from the bottom Co/Pd_1 interface, $K_{s1} = 0.49\ \mathrm{mJ/m^2}$, in the Pd_2(10 ML)/Co/Pd_1(24 ML) trilayers. This may be possible because small strains in the top Co layers were not taken into account. The distribution of the strains in Co from the top Pd_2/Co interface could not be measured by RHEED, and therefore these strains were neglected. However, they may make a small contribution to the PMA. Hence, the energy of IMA, K_{s2}, contains the magneto-elastic contribution, which may confer asymmetry to the K_{s1} and K_{s2} energies. The results of fitting also demonstrate a dependence of the IMA anisotropy K_{s1} from the bottom Co/Pd_1 interface on the thickness of the Pd_1 bottom layer. The changes in IMA are quite small, from 0.36 to 0.49 $\mathrm{mJ/m^2}$, when the thickness of the Pd_1 layer increases from 5 to 24 ML. This may be related to the dependence of IMA on the strains. According to the results of electronic structure calculations, positive strains will increase the IMA of the Co/Pd(111) interface [43].

Although the IMA from the top Pd_2/Co interface is only slightly larger than the IMA from the bottom Co/Pd_1 interface, the bottom Co/Pd_1 interface makes a larger contribution to the PMA than the top Pd_2/Co interface, due to the asymmetry of the strains. The bottom Co layers are more strained than the top Co layers, which are almost fully relaxed. This asymmetry of strains manifests strongly in rather thick Co films. Here, $K_{s1} + K_{s,\mathrm{MEA}} = 1.31\ \mathrm{mJ/m^2}$, while $K_{s2} = 0.64\ \mathrm{mJ/m^2}$ in Pd_2(10 ML)/Co($t_{\mathrm{Co}} > 15$ ML)/Pd_1(24 ML) trilayers. In ultrathin Co films with a thickness of several monolayers, the strains in the top layers do not relax sufficiently, and the asymmetry of the stress is manifested less.

V. CONCLUSIONS

The origin of PMA in epitaxial Pd/Co/Pd(111) trilayered films was experimentally investigated. A model for the calculation of MEA using the experimentally measured thickness distribution of the strains in Co films was proposed and successfully applied. This work discussed the PMA in the Pd/Co/Pd trilayers from two main origins: electronic effects at Co/Pd interfaces and strains in Co films due to lattice mismatch. It was found that both of these origins make comparable contributions to the PMA in Pd/Co/Pd trilayers. The MEA contribution to the total PMA depends on the thicknesses of the Co layer and the Pd bottom layer and may be precisely controlled. The bottom Co layers make the most significant contribution to MEA because the bottom Co layers are more strained than the top Co layers. The values of IMAs from the bottom Co/Pd and top Pd/Co interfaces are comparable with each other. The roughness of the interfaces does not have a large influence on the energy of PMA in these epitaxial Pd/Co/Pd trilayers.

ACKNOWLEDGMENTS

This research was funded by the Russian Ministry of Education and Science (Contract 14.575.21.0039 (RFMEFI57514X0039)).

[1] D. A. Gilbert, B. B. Maranville, A. L. Balk, B. J. Kirby, P. Fischer, D. T. Pierce, J. Unguris, J. A. Borchers, and K. Liu, Nat. Commun. **6**, 8462 (2015).

[2] S. Parkin and S.-H. Yang, Nat. Nanotechnol. **10**, 195 (2015).

[3] K. L. Wang, J. G. Alzate, and P. Khalili Amiri, J. Phys. D. Appl. Phys. **46**, 074003 (2013).

[4] K. Chesnel, A. Safsten, M. Rytting, and E. E. Fullerton, Nat. Commun. **7**, 11648 (2016).

[5] J. M. Shaw, W. H. Rippard, S. E. Russek, T. Reith, and C. M. Falco, J. Appl. Phys. **101**, 023909 (2007).

[6] M. Gottwald, K. Lee, J. J. Kan, B. Ocker, J. Wrona, S. Tibus, J. Langer, S. H. Kang, and E. E. Fullerton, Appl. Phys. Lett. **102**, 052405 (2013).

[7] P. F. Carcia, A. D. Meinhaldt, and A. Suna, Appl. Phys. Lett. **47**, 178 (1985).

[8] M. L. Neel, J. Phys. Radium **15**, 225 (1954).

[9] G. H. O. Daalderop, P. J. Kelly, and M. F. H. Schuurmans, Phys. Rev. B **50**, 9989 (1994).

[10] P. Bruno and J.-P. Renard, Appl. Phys. A **49**, 499 (1989).

[11] S. K. Kim and S. C. Shin, J. Appl. Phys. **89**, 3055 (2001).

[12] M. Kim, S. Kim, J. Ko, and J. Hong, Appl. Phys. Lett. **106**, 102404 (2015).

[13] N. Go, K. Suzuki, and S. Emoto, Key Engin. Mater. **534**, 7 (2013).

[14] S. Nakagawa and H. Yoshikawa, J. Magn. Magn. Mater. **287**, 193 (2005).

[15] C. W. Barton, T. J. A. Slater, R. M. Rowan-Robinson, S. J. Haigh, D. Atkinson, and T. Thomson, J. Appl. Phys. **116**, 203903 (2014).

[16] F. J. A. den Broeder, W. Hoving, and P. J. H. Bloemen, J. Magn. Magn. Mater. **93**, 562 (1991).

[17] B. N. Engel, C. D. England, R. A. Van Leeuwen, M. H. Wiedmann, and C. M. Falco, J. Appl. Phys. **70**, 5873 (1991).

[18] S. T. Purcell, H. W. Van Kesteren, E. C. Cosman, W. B. Zeper, and W. Hoving, J. Appl. Phys. **69**, 5640 (1991).

[19] B. N. Engel, C. D. England, R. A. Van Leeuwen, M. H. Wiedmann, and C. M. Falco, Phys. Rev. Lett. **67**, 1910 (1991).

[20] A. Maesaka and H. Ohmori, IEEE Trans. Magn. **38**, 2676 (2002).

[21] S.-K. Kim, V. A. Chernov, and Y.-M. Koo, J. Magn. Magn. Mater. **170**, L7 (1997).

[22] A. Yamaguchi, S. Ogu, W. H. Soe, and R. Yamamoto, Appl. Phys. Lett. **62**, 1020 (1993).

[23] A. Hallal, H. X. Yang, B. Dieny, and M. Chshiev, Phys. Rev. B **88**, 184423 (2013).

[24] H. Almasi, D. R. Hickey, T. Newhouse-Illige, M. Xu, M. R. Rosales, S. Nahar, J. T. Held, K. A. Mkhoyan, and W. G. Wang, Appl. Phys. Lett. **106**, 182406 (2015).

[25] A. Kaidatzis, C. Bran, V. Psycharis, M. Vázquez, and J. M. García-Martín, Appl. Phys. Lett. **106**, 262401 (2015).

[26] W. X. Wang, Y. Yang, H. Naganuma, Y. Ando, R. C. Yu, W. X. Wang, Y. Yang, H. Naganuma, Y. Ando, R. C. Yu, and X. F. Han, Appl. Phys. Lett. **99**, 012502 (2012).

[27] Y. P. Ivanov, A. I. Ilin, A. V. Davydenko, and A. V. Zotov, J. Appl. Phys. **110**, 083505 (2011).

[28] A. V. Davydenko, A. G. Kozlov, A. V. Ognev, M. E. Stebliy, and L. A. Chebotkevich, Appl. Surf. Sci. **384**, 406 (2016).

[29] C. J. Howe, M. D. Cropper, R. M. Wardle, P. Bailey, and T. C. Q. Noakes, Surf. Sci. **604**, 1658 (2010).

[30] J. T. Kohlhepp, G. J. Strijkers, H. Wieldraaijer, and W. J. M. de Jonge, Phys. Status Solidi A **189**, 701 (2002).

[31] A. Atrei, G. Rovida, M. Torrini, U. Bardi, M. Gleeson, C. J. Barnes, and V. G. Capponi, Surf. Sci. **372**, 91 (1997).

[32] M. Wasniowska, N. Janke-Gilman, W. Wulfhekel, M. Przybylski, and J. Kirschner, Surf. Sci. **601**, 3073 (2007).

[33] S. T. Purcell, H. W. van Kesteren, E. C. Cosman, and W. Hoving, J. Magn. Magn. Mater. **93**, 25 (1991).

[34] S. Boukari, E. Beaurepaire, H. Bulou, B. Carrière, J. P. Deville, F. Scheurer, R. Baudoing-Savois, and M. De Santis, Surf. Sci. **430**, 37 (1999).

[35] F. J. A. den Broeder, H. C. Donkersloot, H. J. G. Draaisma, and W. J. M. de Jonge, J. Appl. Phys. **61**, 4317 (1987).

[36] G. R. Harp, S. S. P. Parkin, R. F. C. Farrow, R. F. Marks, M. F. Toney, Q. H. Lam, T. A. Rabedeau, and R. J. Savoy, Phys. Rev. B. **47**, 8721 (1993).

[37] A. M. N. Niklasson, B. Johansson, and H. L. Skriver, Phys. Rev. B. **59**, 6373 (1999).

[38] H. Sakurai, F. Itoh, Y. Okabe, H. Oike, and H. Hashimoto, J. Magn. Magn. Mater. **198-199**, 662 (1999).

[39] A. Bach Aaen, E. Lægsgaard, A. Ruban, and I. Stensgaard, Surf. Sci. **408**, 43 (1998).

[40] A. Canzian, H. O. Mosca, and G. Bozzolo, Surf. Sci. **551**, 9 (2004).

[41] H. Takahashi, S. Tsunashima, S Iwata, and S. Uchiyama, J. Magn. Magn. Mater. **126**, 282 (1993).

[42] C. H. Lee, H. He, F. J. Lamelas, W. Vavra, C. Uher, and R. Clarke, Phys. Rev. B **42**, 1066 (1990).

[43] R. H. Victora and J. M. MacLaren, Phys. Rev. B **47**, 11583 (1993).